The Effects of Control System Stiffness Models on the Dynamic Stall Behavior of a Helicopter

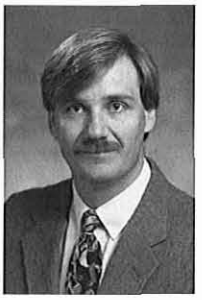

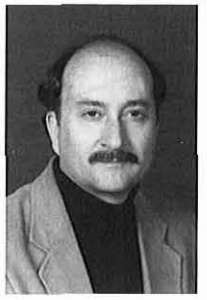

Robert M. Kufeld
Aerospace Engineer

Wayne Johnson

NASA Ames Research Center, Moffett Field, California

The control system stiffness of an UH–60A helicopter was measured. A description of the measurements and the results is provided. The measured control system stiffness values were used within a comprehensive analysis, CAMRAD II, to establish a baseline calculation of the rotor system during an extreme thrust condition causing dynamic stall on the rotor. A validation of the baseline CAMRAD II model was made by comparing to measured blade shake test data and level-flight, high-thrust, flight-test data also showing dynamic stall from the UH–60A Airloads Program. Finally, an evaluation of the sensitivity of the rotor system response to different control system stiffness models was made. The calculated results indicate a moderate level of sensitivity to changes of control system stiffness in the presence of dynamic stall. This finding in itself is an important determination, as this paper narrows the range of possibilities, which are assumed to be important to dynamic stall predictions by demonstrating the effects of control system stiffness on predictions and thereby moving researchers to focus on other attributes such as three-dimensional aerodynamics.

Notation

b	number of blades
C_w/σ	weight coefficient, $\frac{GW}{\pi\sigma\rho\Omega^2R^4}$
c	blade chord, ft
GW	aircraft gross weight, lb
K	structural stiffness, ft-lb/deg.
R	rotor radius, ft
r	radial location, ft
μ	advance ratio
ρ	air density, slug/ft^3
σ	rotor solidity, $bc/\pi R$
Ω	rotor speed, rad/sec

Introduction

Accurately predicting the dynamic stall characteristics of a helicopter rotor is one of the major goals of the rotorcraft industry; loads caused by this condition are very important as they are used to size the helicopter control system. This prediction requires accurate models of the rotor structure, helicopter control system, linear and nonlinear aerodynamics and inflow. Bousman (Ref. 1), has taken a step to improve understanding of dynamic stall through a qualitative examination of UH–60A helicopter flight test data acquired during the NASA/Army UH–60A Airloads Program (Ref. 2). One of Bousman's conclusions was that the locations of the dynamic stall events occur in a consistent pattern in terms of azimuth and radial station and are probably controlled by the torsional dynamics of the blade. A key parameter required to predict the torsional dynamics of a blade, helicopter control system stiffness, is often difficult to measure and calculate accurately. In most cases, the value of the control system stiffness is only estimated after flight testing when the measured value of the blade torsional frequency can be used to validate the calculations.

The control system stiffness of the UH–60A Airloads Program aircraft was measured at Ames Research Center. A description of the experimental setup and results are included within this paper. The measured control system stiffness value was used to establish a new analytical model of the rotor system. The comprehensive rotorcraft code, CAMRAD II, (Refs. 3, 4), was used to calculate the baseline results of the new model for validation with the flight test data collected during the NASA/Army UH–60A Airloads Program and with the non-rotating blade frequency data measured in a shake test by Hamade and Kufeld (Ref. 5). Finally, with the fidelity of the comprehensive code established, the sensitivity of blade torsional frequencies and the rotor system response during dynamic stall to different control system stiffness models was evaluated.

UH–60A Swashplate and Stationary Links

A description of the UH–60A swashplate and stationary links geometry is useful for interpreting the measured results to follow. Figure 1 shows a schematic of the location of the UH–60A stationary swashplate links with respect to the rotor azimuth. The three stationary links are located unevenly around the azimuth. The three links are arranged with 90° between each of them leaving half of the swashplate unsupported for the full 180°. The UH–60A main rotor has a leading edge pitch link which, when aligned with the forward stationary link, positions the blade spindle at the 90° rotor azimuth position. With the links 90° apart, the pitch links for the next two blades will also be aligned with stationary links at the 180° and 270° azimuth position.

Figure 2 shows a cut-away view of the UH–60A control system between the primary servos and the swashplate with the three stationary links labeled. Notice that the distance between the forward and lateral

Presented at the American Helicopter Society 54th Annual Forum, Washington, D.C., May 20–22, 1998. Manuscript received January 1999; accepted June 2000.

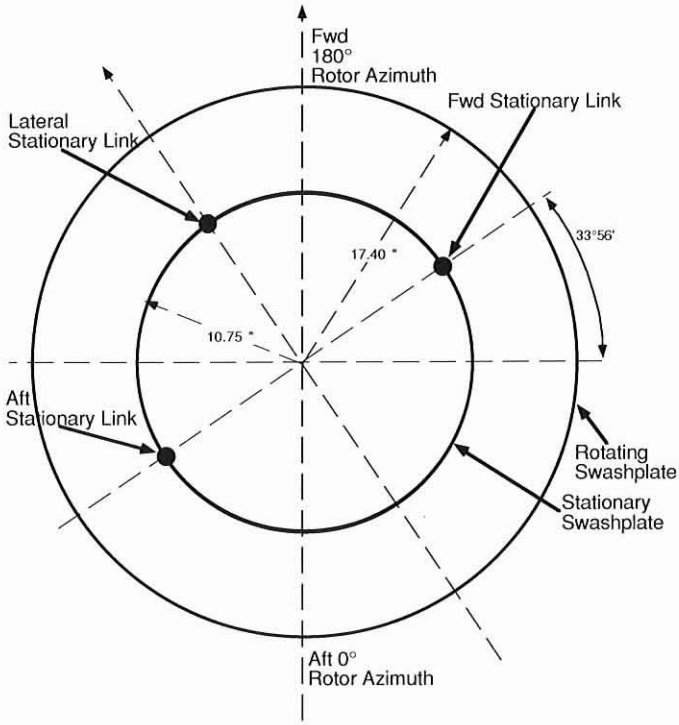

Fig. 1. Schematic of the UH–60A swashplate stationary link location.

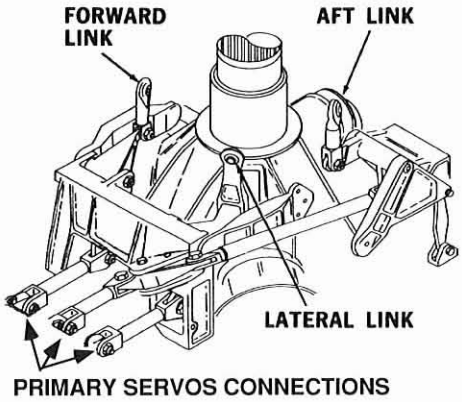

Fig. 2. Cut away view of UH–60A control system linkages.

stationary links to the primary servos is essentially the same; however, the aft stationary link has one additional component within its series that is significantly longer than the linkages found in the other two stationary link systems.

Control Stiffness Measurement

Set-up

A measurement of the control stiffness of the UH–60A Airloads Program helicopter was made at Ames Research Center. This is the same aircraft that was used for the NASA/Army Airloads Program. Figure 3 shows a photo of the test set up with the hardware labeled. For this test all four blades were removed and spindle adapter blocks were designed, manufactured, and installed into the blade attachment spindle using the blade attachment pins. The adapter blocks served three functions. First, they served as the loading interface to the control system. A leading-edge-

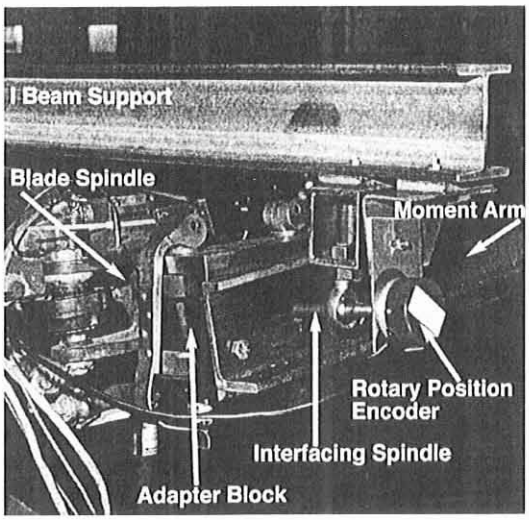

Fig. 3. Photo of UH–60A blade spindle with control system stiffness hardware attached.

down pitching moment was applied to each of the four blade spindles by a six-foot moment arm attached to the adapter block. Up to 264 lb of dead weight was applied. Secondly, the rotation of the blade spindle was measured with a 16 bit rotary encoder with a resolution of .0055 degree attached to the adapter block via a load bearing interfacing spindle. Thirdly, the adapter block was used to position the blade spindle to approximately 6° flap up and 7° lag aft to simulate the position of the blade spindle during flight. To do this the interfacing spindle was passed through a rod end attached to an I-beam support structure mounted to the top of the hub. This configuration not only fixed the flap and lag position of each blade while allowing a full range of pitch motion, but also reacted most of the vertical shear load of the dead weight and transferred it to the transmission drive shaft.

In addition to the four rotary encoders, the loads of all four pitch links were measured with strain gages, and the positions of the three primary servos were measured with string potentiometers. The pitch link loads were monitored to ensure limits loads were not exceeded during testing. Any movement of the primary servos was converted to pitch deflection of the blade spindles and added to the measured spindle rotations as a correction during data processing.

Testing procedure

The aircraft was powered with an external power unit and the aircraft's hydraulic pump was turned on to simulate normal operation during flight. To fix the controls in a repeatable position for each measurement, the flight control rigging pins were installed in all four of the control axes. Although the rigging pins allow for a fixed and repeatable position of the swashplate during each loading run, the ideal test condition, with all blade spindles at the same pitch attitude, could not be obtained because the rigged position was not at neutral cyclic. The 90° rotor azimuth position of the blade spindle was selected as the baseline position. As mentioned above, this corresponds to a pitch link aligned with the forward stationary link of the stationary swashplate. Changes in azimuth positions from this baseline were measured with a transit mounted on top of the hub.

Measurements were made on all four blades simultaneously. The spindle loading was done manually with calibrated weights. The nominal load sequence started with a preload of 44 lb, moved up to 264 lb in 22 lb increments, and then back down to 44 lb, for a total of 21 measurements.

This applied a maximum nose down pitching moment on the control system of 1824 ft-lb including the 44 lb preload and the weight of the moment arm, 80 lb. Four different loading conditions were used:

1) Collective Loading: all four blade spindles were loaded simultaneously in the same direction from 44 to 264 lb.

2) Reactionless Loading: all blades spindles started with 154 lb load; two opposite spindles (e.g. blades at 0° & 180°) increased their loading to 264 lb while the other set of opposite spindles (e.g. 90° & 270°) decreased their loading to 44 lb.

3) Cyclic Loading 1: again starting with 154 lb on all four blade spindles; the loading only changed on one set of opposite blades (e.g. 0° & 180°). Loading on one blade increased to 264 lb while the loading on the opposite blade decreased to 44 lb. The load on the 90° & 270° blade spindle remained constant.

4) Cyclic Loading 2: same as above, but the loading changes were performed on the other two blade spindles (e.g. 90° & 270°). The load on the 0° & 180° blade spindle remained constant.

Once a loading cycle was completed, the hub was rotated 15° to a new azimuth position and the loading cycle was repeated. The loading was performed at seven different azimuth positions to cover the full rotation of the rotor. The first and last azimuth positions tested provided a set of repeated data measurements, except for a shift of 90° by the rotor hub.

Experimental Results

Following the tests, the spindle angle data were corrected for movement of the primary servos and the loading was corrected for non-zoo blade spindle angles. Figure 4 shows a typical example of the measured results. In most cases the blade spindle deflection showed significant hysteresis, most likely caused by friction in the numerous rod ends in the control system, but the deflection usually returned to the starting value at the end of the loading sequence. The slope of a least squares curve fit provided a linear representation of the data that approximated the control system stiffness of a single blade at a particular azimuth position. It is expected that most of the hysteresis would be removed by the control system dither created in the flight environment, thus justifying a linear model.

The measured stiffnesses are unique functions of the rotor azimuth and the loading condition as is shown in Fig. 5. Comparing the measured results to the physical arrangement of the UH–60A swashplate and control links (Fig. 1) improves the confidence of the measurements. As expected, the largest stiffness for the collective loading mode (Fig. 5(a)) occurs at a blade position near 180°, where the pitch link is aligned with the lateral stationary link and the aft and forward stationary link are only 90° away. Conversely, the lowest stiffness occurs at a blade position of 360°, which is the farthest point away from a stationary link.

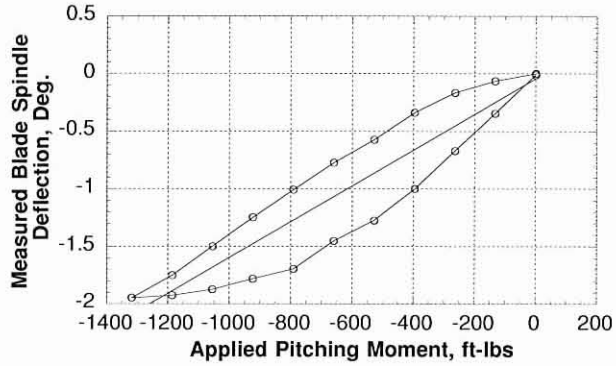

Fig. 4. Typical example of loading hysteresis for collective loading of a single blade spindle; spindle at 285° azimuth.

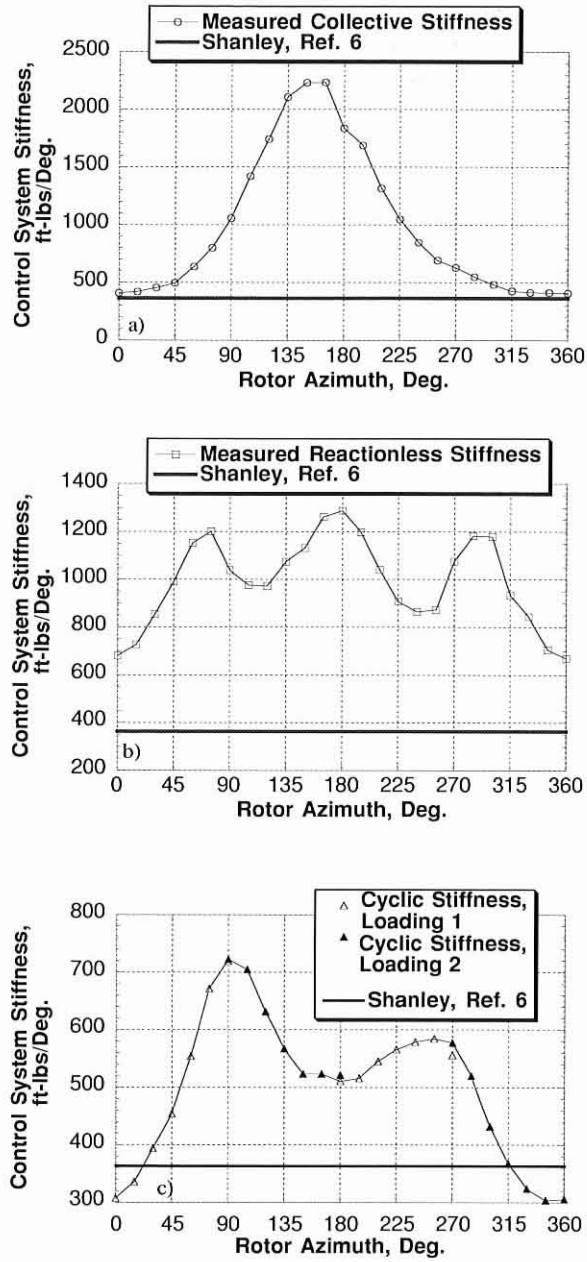

Fig. 5. Measured individual blade stiffness as a function of rotor azimuth for (a) collective, (b) reactionless, and (c) cyclic loading compared with Reference 6.

The reactionless loading (Fig. 5(b)) attempts to isolate the stiffness of the pitch links by keeping a constant load on the swashplate and primary servos. This results in a smaller variation of stiffnesses with azimuth. The location of the primary servos is also apparent, as the pitch links appear stiffer in the vicinity of the servos.

To better understand the shape of the control system stiffness due to cyclic loading (Fig. 5(c)), remember that the loading was done in pairs (90° & 270° and 180° & 360°). The stiffness near the 90° & 270° azimuth positions should be higher because two of the stationary links are involved

while the stiffness near 180° & 360° azimuth position should be lower because only one stationary link is involved. In addition, the stiffness near 360° is much lower compared to 180° because the stationary links are far away from this azimuth position. Referring back to Fig. 2, remember that the aft stationary link (blade spindle near the 270° rotor azimuth position) has one additional component within its linkage. This long link has the effect of reducing the stiffness near the aft link (270° azimuth) and this is seen in Fig. 5(c).

Also shown in Fig. 5 is the published UH–60A control system stiffness from Ref. 6 (363 ft-lb/deg.). This previously published value is seen to be considerably in error for all 4 loading conditions, although the published value does match the current experimental data for collective stiffness near 0° azimuth. (This difference is further assessed a bit later).

Control Stiffness Model

To use the above information in the comprehensive analysis program, CAMRAD II, the measured control system stiffness in the rotating frame was converted to control system stiffness in the non-rotating frame using the multi-blade coordinate transformation. The equations below taken from Ref. 7 describe the transformation.

$$K_{col} = \frac{1}{N}\sum_{m=1}^{N} K^{(m)}$$

$$K_{cos} = \frac{2}{N}\sum_{m=1}^{N} K^{(m)} \cos \psi_m$$

$$K_{sin} = \frac{2}{N}\sum_{m=1}^{N} K^{(m)} \sin \psi_m$$

$$K_{react} = \frac{1}{N}\sum_{m=1}^{N} K^{(m)}(-1)^m$$

where $K^{(m)}$ is the measured stiffness for the mth blade, ψ_m is the azimuth position of the mth blade, and N is the number of blades.

The transformation was performed for each of the four different loadings described above. Figure 6 shows the transformed values of the primary stiffness for each of the seven different azimuthal loadings. As expected, the coordinate transformation provides fixed system stiffnesses generally independent of azimuth. As such, average values of the stiffnesses were calculated from the seven different azimuth positions measured. The (4 × 4) matrix shown below represents the average fixed system stiffness measured during testing.

$$\begin{Bmatrix} M_{col} \\ M_{cos} \\ M_{sin} \\ M_{rea} \end{Bmatrix} = \begin{bmatrix} 897 & -135 & 57 & -32 \\ -357 & 535 & -13 & -14 \\ 128 & 1 & 698 & -53 \\ -53 & 18 & -15 & 1090 \end{bmatrix} \begin{Bmatrix} \theta_{col} \\ \theta_{cos} \\ \theta_{sin} \\ \theta_{rea} \end{Bmatrix}$$

For the calculated results presented in this paper the off-diagonal terms of the fixed system control stiffness are set equal to zero. Only the diagonal terms are used to model the UH–60A control system stiffness as the off-diagonal term are relatively small and most comprehensive rotorcraft codes are not set-up for such a complex stiffness model.

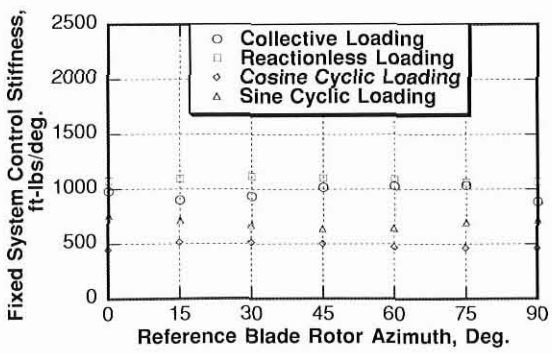

Fig. 6. Diagonal elements of the fixed system control stiffness as a function of the reference blade azimuth position.

UH–60A Math Model

The model used for the calculations performed in this paper was a modified version of the model Bousman and Maier (Ref. 8), used in an earlier study with CAMRAD/JA. The modifications include changes in format to be compatible with the CAMRAD II input format. The actual UH–60A Airloads instrumented blades were modeled. This results in minor decreases in the blade flapwise and edgewise stiffness because the pressure instrumented blade was manufactured without the nickel abrasion strip on the outboard portion of the blade. A minor change to the blade's center of gravity was made because of the instrumentation wires added to the leading edge of the blade. Lastly, a change to the aerodynamic twist of the SC1094 R8 airfoil section of the blade was made to be consistent with the description of the chord line for that airfoil.

To verify the results of the new structural blade model, a comparison was made of the non-rotating blade frequencies calculated by CAMRAD II with the measured shake test results (Ref. 5). Minor modifications of the CAMRAD II model enabled the calculation of non-rotating blade frequencies with the blade suspended by bungee cords from the root, very similar to the shake test configuration. Table 1 summarizes the results of this comparison.

To accurately calculate these high frequency non-rotating modes, the blade was modeled using eight beam elements. For rotating-mode calculations it was sufficient to use three beam elements.

The airfoil tables used by Bousman and Maier (Ref. 8) were also slightly modified to correct for some non-typical behavior within them. Lim (Ref. 9), first applied these modifications to the SC1095 airfoil deck and similar changes were made to the SC1094 R8 airfoil deck used here.

Within the CAMRAD II comprehensive analysis model, the control system can be modeled with different levels of sophistication or complexity. For this study, two modeling approaches were evaluated. A simple model using only one spring for the pitch links (rotating system representation of the control system stiffness) was evaluated first. A more complete model for the pitch link/swashplate (fixed system representation

Table 1. Comparison of measured and calculated non-rotating blade frequencies

Blade mode	Shake test	CAMRAD II	Per cent error
1st Flap	4.69 hz	4.44 hz	5.3
2nd Flap	12.46	12.60	1.1
3rd Flap	24.87	25.44	2.3
1st Chord	25.55	25.07	1.9
4th Flap	40.51	39.93	1.4
1st Torsion	44.49	46.11	3.6
5th Flap	62.28	65.52	5.2
2nd Chord	67.37	68.36	1.5

of the control system stiffness) was also evaluated. The fixed system representation of the control system stiffness consists of four springs. A linear spring and two angular springs in the non-rotating frame, to model the collective and cyclic stiffnesses respectively of the swashplate motion, plus a linear spring in the pitch link to model the reactionless stiffness.

One final conversion of the diagonal elements of the linearized stiffness matrix was required to obtain the proper values for the CAMRAD II model. The values of the stiffness matrix shown above were derived from measurements of the control system stiffness at the pitch bearing. The values of the spring models used within CAMRAD II were derived from the diagonal elements of the pitch bearing stiffness measurements using the geometry of the test setup. The pitch link stiffness is a function of the measured reactionless stiffness. The swashplate collective stiffness is a function of the measured collective stiffness in series with the pitch link stiffness. The swashplate lateral stiffness is a function of measured cosine stiffness in series with the pitch link stiffness. The swashplate longitudinal stiffness is a function of the measured sine stiffness in series with the pitch link stiffness.

Baseline Dynamic Stall

The first objective of the CAMRAD II analysis was to correlate a baseline calculation using the rotating control system stiffness model with flight test data capturing the dynamic stall phenomenon. The second objective was to evaluate the sensitivity of the rotor response to variations in the rotating control system stiffness model. Finally, the fixed system control stiffness representation, a four-spring control system stiffness model, was inserted into CAMRAD II to evaluate the sensitivity of the rotor response to a simple and a complex control system stiffness model.

The baseline flight test data was selected from the UH–60A Airloads Flight Test Program. The Program collected a comprehensive set of level flight data points. They covered six different thrust coefficients, (approximately $C_w/\sigma = 0.08$ to 0.13 in 0.01 increments) within the power-limit speed boundaries of the helicopter (advance ratio between 0.0 and 0.37). From these data a small set of 6 test conditions (called counters within the Airloads database) were selected to show the effects of rotor thrust on the dynamic stall of this rotor system at a constant advance ratio = 0.23. Figure 7 shows the measured blade pitching moment at $r/R = 0.865$ vs azimuth for each of the different thrust values. The flight pressure data shown has been decimated from a measured azimuth resolution of approximately 1.5° to 8° without affecting the conclusions drawn in this paper as the CAMRAD II azimuth resolution is equal to 15°. A rapid decrease and recovery of the section pitching moment usually indicates the occurrence of dynamic stall. Here two dynamic stall cycles are clearly seen at 270° and 345° azimuth for the two highest thrust conditions measured. Based on these flight data, the CAMRAD II calculation will be compared to test condition Counter 9017 with a thrust value of $C_w/\sigma = 0.13$.

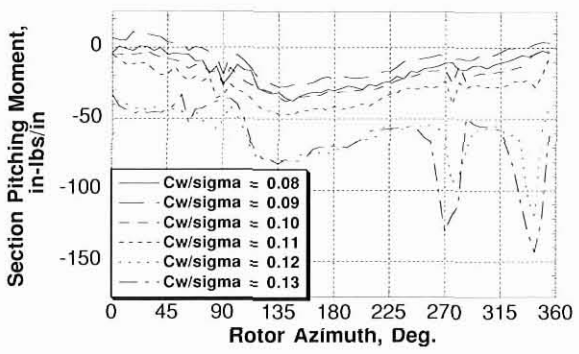

Fig. 7. Measured blade section pitching moment as a function of rotor azimuth for different values of C_w/σ, r/R = 0.865, $\mu = 0.23$.

For the baseline calculations the control system stiffness was modeled with a simple one-spring stiffness model equivalent to the measured reactionless stiffness of 1090 ft-lb/deg. The calculations were made with wind tunnel trim, a free wake, and the Leishman-Beddoes' dynamic stall model (Ref. 10). The thrust and once-per-revolution flapping were trimmed to the values measured in the flight test, with the shaft angle and other operating condition variables fixed at the measured values. CAMRAD II was run to match the different level flight conditions of $C_w/\sigma = 0.12$ and 0.13. The results are shown in Fig. 8 which compares the calculated values of blade flap bending at $r/R = 0.30$, pitch link load, and blade section pitching moment at $r/R = 0.865$ to the flight test data from Counter 9017. The steady values of the structural parameters have been removed from both the calculated and flight test data to ease comparison because of poor correlation.

Comparing the calculated and measured results it is seen that the wave forms of all three parameters have very similar shapes if the higher frequency content of the flight data is over looked, but the overall magnitude of the calculated values for the pitch link load and blade section pitching moment is much lower than the measured. The high frequency oscillations in both the pitch link load and flap bending measurements are apparently not associated with stall, since they begin in the second quadrant of the disk. Bousman (Ref. 1), showed that for this case the first stall cycles begins at around 225° azimuth on the inboard part of the blade, reaching the tip at around 290°. Additionally, a major difference between the calculated and measured results is the absence of the second dynamic stall cycle as shown in Figure 8(f).

To get a better correlation of the magnitude of the loads from the calculations, the trim procedure of the analysis was slightly changed. Additional runs were made so that the analysis would hold a fixed collective and adjust trim to the measured flapping. Four more runs at different collectives between 13° and 16° were made. These calculations are also shown in Fig. 8. These results still closely match the thrust level of the flight test condition as the rotor has reached its thrust limit and changes very little with increasing collective. The effects of increasing collective are an increase in loading on the plotted parameters and the movement of the dynamic stall cycle forward from 255° to about 195°. There is also indication that a second dynamic cycle follows the first and that the airflow does not return to an unstalled state until late in the fourth quadrant.

After reviewing the above data it was determined that the calculations with a collective setting equal to 13 degrees provided the best option to compare with different values of control system stiffness. The magnitude of the pitch link loading is closer to the flight value, and the blade section pitching moment still shows the major stall event to occur near 255° azimuth. Higher values of collective increase the pitch link loading closer to flight values, but make major changes to the initiation of the dynamic stall cycle.

Control Stiffness Variation

The value of the simple (one spring) control system stiffness model was changed to see its effect. The different values selected cover the range from 363 ft-lb/deg. [Ref. 6], to 1090 ft-lb/deg., the measured reactionless mode stiffness. Two intermediate values of control system stiffness were selected that match the two measured cyclic stiffness values of 535 ft-lb/deg. and 698 ft-lb/deg. These values provide a relatively even increment over the given range to evaluate the effect of control system stiffness.

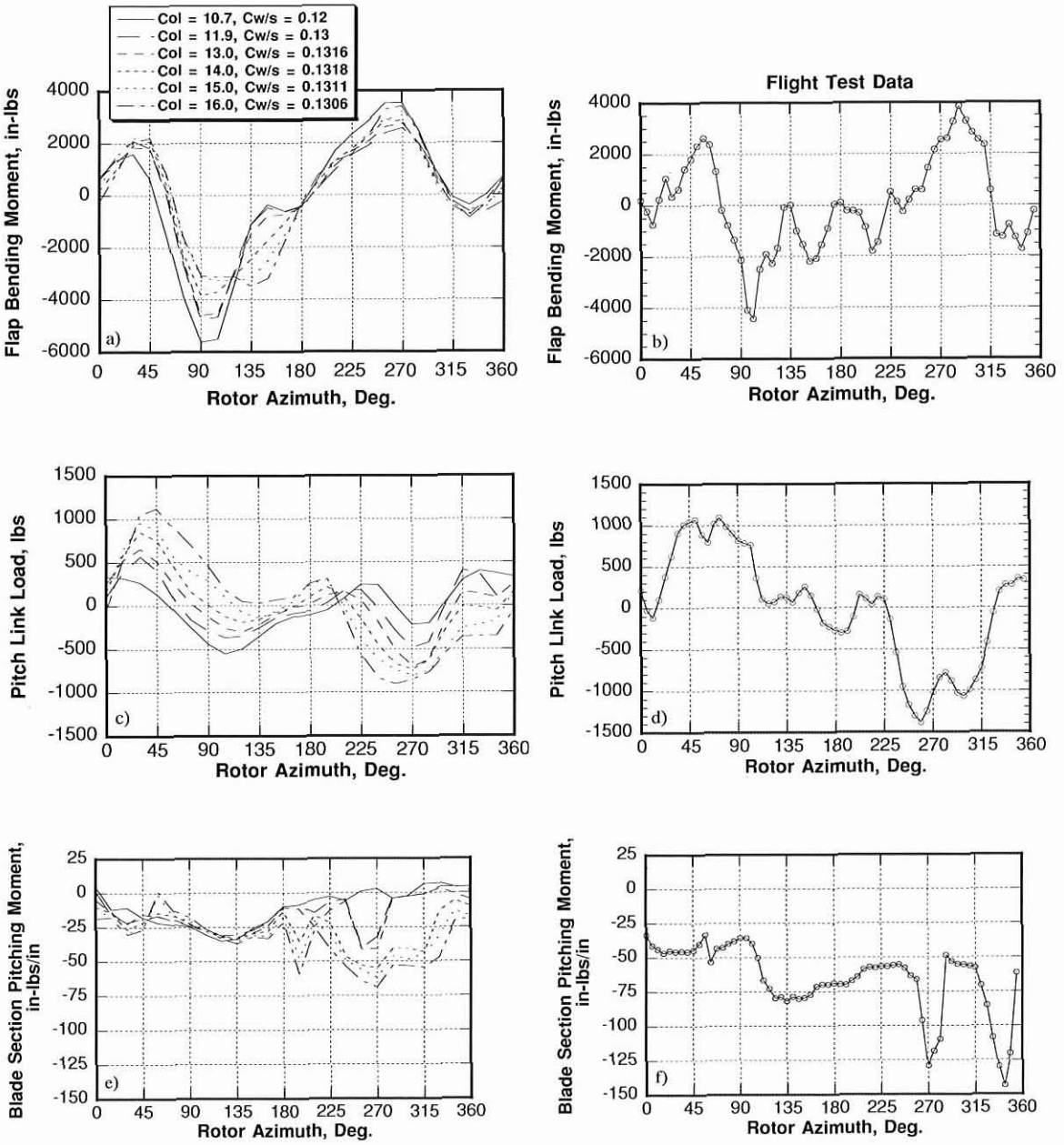

Fig. 8. Calculated and measured flight test data for: (a,b) flap bending, r/R = 0.30, steady removed; (c,d) pitch link load, steady removed; and (e,f) blade section pitching moment, r/R = 0.865; trimmed to rotor thrust or collective setting. (Counter 9017, $\mu = 0.23$).

Figure 9 shows the calculated blade pitch/torsion frequency at the nominal UH–60A rotor speed as a function of the measured control system stiffness. For the range shown, between the Ref. 6 value of control system stiffness to the maximum stiffness measured for reactionless loading, the variation in blade frequency is about 10%.

Figure 10 shows the rotor response to the four different simple control system stiffness models plus the complex four-spring control system stiffness model. There is very little change in the flap bending moment calculation over the full range of control system stiffness values. Since both pitch link load and the section pitching moment are strongly influenced by the blade torsional dynamics a bigger change is expected in these two parameters. Figure 10 shows an increase in peak-to-peak pitch link loads from ±400 lb to ±700 lb, as control system stiffness is increased. At the lowest value of control system stiffness (Ref. 6), the blade section pitching moment does not indicate stall, but a dynamic

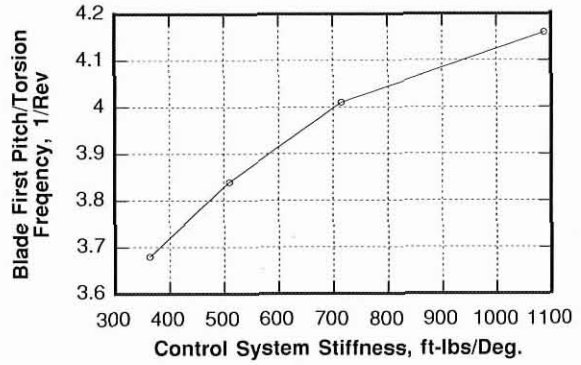

Fig. 9. Calculated pitch/torsion mode frequencies at nominal rotor speed as a function of measured control system stiffness.

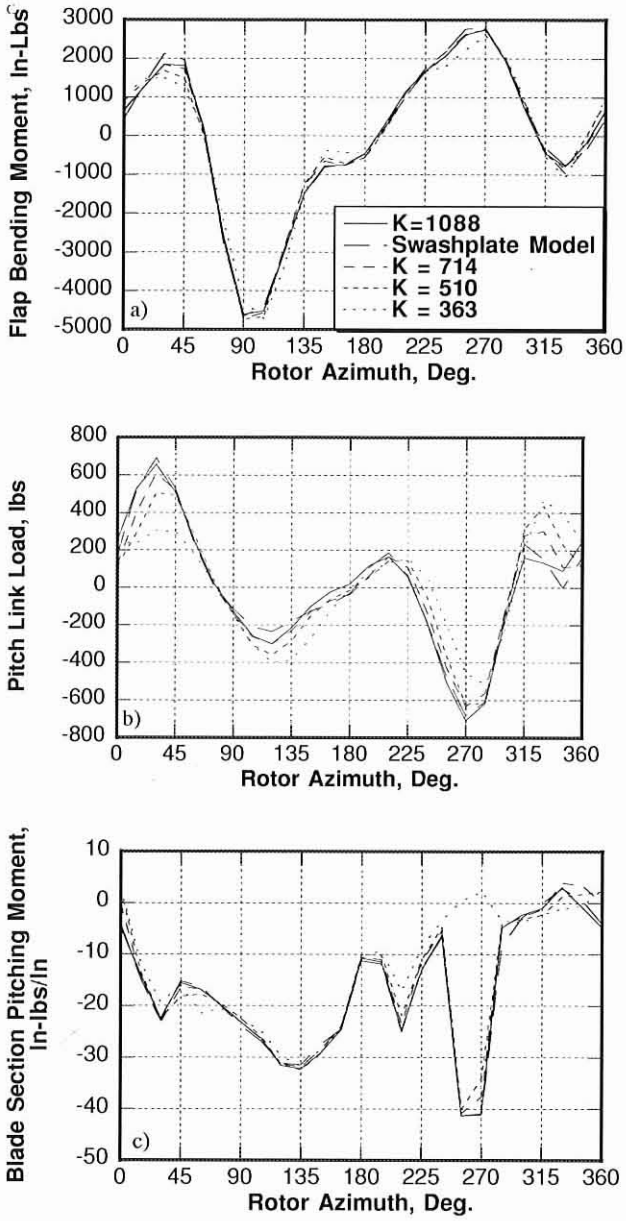

Fig. 10. Calculated values of (a) blade normal flapping at r/R = 0.30, (b) pitch link load, and (c) blade section pitching moment at r/R = 0.865 as a function of rotor azimuth for different models of control system stiffness, $C_w/\sigma = 0.13$, $\mu = 0.23$.

stall cycle is observed for higher stiffness. Figure 10 shows little change in value or wave form for the more complex swashplate model suggesting that this complexity is not required for this model.

Concluding Remarks

The control system stiffness of an UH–60A helicopter was measured for four different loading conditions. The measured results were then incorporated into an analytical model compatible with the CAMRAD II comprehensive rotorcraft code. Calculations were performed with a variety of different control system stiffness models to evaluate the sensitivity of rotor parameters to stiffness modeling.

1) The measured collective, cyclic, and reactionless stiffness of the UH–60A swashplate vary considerably from each other and are higher than the value shown in Ref. 6.

2) The measured stiffness behavior with azimuth is directly related to the swashplate and fixed system servo orientation.

3) Conversion of the individual stiffness measurements from the rotating system to the fixed system substantially removes the azimuthal dependence.

4) The CAMRAD II analytical model shows qualitative agreement with the measured oscillatory rotor loads. The predicted peak-to-peak pitch link loads and torsional moments are consistently smaller than test values. Pitch link load correlation is best at highest collective, but the section pitching moment shows too much stall behavior in the fourth quadrant at this collective setting. The best overall match to the baseline flight condition is for a collective setting of 13°.

5) The evaluation of the simple control system model in CAMRAD II indicates that the measured values of control system stiffness improves pitch link load correlation over the value specified in Ref. 6.

6) The evaluation of the complex swashplate and the simple stiffness models in CAMRAD II indicates that the complex model does not improve the prediction of dynamic stall.

References

[1]Bousman, W. G., "A Qualitative Examination of Dynamic Stall from Flight Test Data," American Helicopter Society 53rd Annual Forum Proceedings, Virginia Beach, VA, April 29–May 1, 1997.

[2]Kufeld, R. M., Balough, D. L., Cross, J. L., Studebaker, K. F., Jennison, C. D., and Bousman, W. G., "Flight Testing of the UH–60A Airloads Aircraft," American Helicopter Society 50th Annual Forum Proceedings, Washington, D.C., May 11–13, 1994.

[3]Johnson, W., "Technology Drivers in the Development of CAMRAD II," American Helicopter Society Aeromechanics Specialists Conference, San Francisco, CA, January 19–21, 1994.

[4]Johnson, W., "Rotorcraft Aerodynamics Models for a Comprehensive Analysis," American Helicopter Society 54th Annual Forum Proceedings, Washington, D.C., May 20–22, 1998.

[5]Hamade, K. S., and Kufeld, R. M., "Modal Analysis of UH–60A Instrumented Rotor Blades," NASA TM 4239, November 1990.

[6]Shanley, J. P., "Application of the Comprehensive Analytical Model of Rotorcraft Aerodynamics and Dynamics to the UH–60A Aircraft," SER-72126, February 1986.

[7]Johnson, W., *Helicopter Theory*, Princeton University Press, Princeton, New Jersey, 1980, Chapter 11.

[8]Bousman, W. G., and Maier, T. H., "An Investigation of Helicopter Rotor Blade Flap Vibratory Loads," American Helicopter Society 48th Annual Forum Proceedings, Washington, D.C., June 3–5, 1992.

[9]Lim, J. W., "Analytical Investigation of UH–60A Flight Blade Airloads and Loads Data," American Helicopter Society 51st Annual Forum Proceedings, Ft. Worth, TX, May 9–11, 1995.

[10]Leishman, J. G., and Beddoes, T. S., "A Semi-Empirical Model for Dynamic Stall," *Journal of the American Helicopter Society*, Vol. 24, (3), July 1989.